communications biology

Article

https://doi.org/10.1038/s42003-024-07410-z

Carbonic anhydrase 2-derived drug-responsive domain regulates membrane-bound cytokine expression and function in engineered T cells

Check for updates

Mara C. Inniss[1], Sean G. Smith[1], Dan Jun Li[1], Benjamin Primack[1], Dexue Sun[1], Grace Y. Olinger[1], Kerri-Lynn Sheahan[1], Theresa Ross[1], Meghan Langley[1], Violet Young[1], Andres Alvarado[1], Shabnam Davoodi[1], Jiefei Geng[1], Michael Schebesta[1], Michelle L. Ols[1], Jeremy Tchaicha[1], Jan ter Meulen[1,2] & Dhruv K. Sethi[1,2]

Adoptive cell therapies (ACT) have shown reduced efficacy against solid tumor malignancies compared to hematologic malignancies, partly due to the immunosuppressive nature of the tumor microenvironment (TME). ACT efficacy may be enhanced with pleiotropic cytokines that remodel the TME; however, their expression needs to be tightly controlled to avoid systemic toxicities. Here we show T cells can be armored with membrane-bound cytokines with surface expression regulated using drug-responsive domains (DRDs) developed from the 260-amino acid protein human carbonic anhydrase 2 (CA2). The CA2-DRD can be stabilized in vitro and in vivo with the FDA-approved small-molecule CA2 inhibitor acetazolamide (ACZ). We develop conditional degrons using library-based screening of mutants and show characterization of one DRD using crystallography and molecular dynamics (MD) simulations. Using protein-engineering solutions to increase the valency of DRDs fused to the cargo we have developed "modulation hubs" and show tight regulation of membrane-bound cytokines IL2, IL12, IL15, IL21, IL23, and IFNα in genetically engineered T cells. Finally, CA2-DRD regulated IL12 mediates regulated efficacy in a solid tumor model. Regulation of pleotropic cytokines potentially paves the way to safely use these powerful cytokines in ACT for cancer treatment.

Adoptive cell therapy (ACT) has revolutionized the treatment of hematologic malignancies but has encountered obstacles in treating solid-tumor malignancies, in part due to the immunosuppressive tumor microenvironment (TME). Expression of powerful immunomodulatory cytokines by genetically engineered T cells represents an attractive approach to overcome the intrinsic resistance of solid tumors to ACT but carries the risk of severe and potentially lethal systemic side effects that need to be safely controlled[1–3]. To this end, "hard-wiring" expression control mechanisms into T cells using synthetic biology have been pursued, including logic-gated expression circuits that require integration of several signals coming from different receptors for downstream gene expression[4]. While conceptually elegant, gene activation and subsequent protein expression are typically not titratable using this technology, and if aberrant signaling occurs then uncontrolled and potentially life-threatening T-cell activation can be stopped only by using engineered cellular kill switches, such as inducible caspase 9 induction with small molecules[5]. Since the in vivo destruction of a possibly life-saving product is neither desirable for the patient nor the payor of a costly treatment, technologies that allow T-cell armoring with fully regulatable cytokines are urgently needed.

Many strategies that are being explored to achieve post-translational control of protein activity through direct physical or chemical stimuli interacting in either a non-covalent or covalent fashion with their target face challenges related to synthesis, delivery, and specificity[6]. Biological tools for post-translational control of protein activity, on the other hand, have the potential to circumvent many of these obstacles. One way of achieving regulation of a target protein is by fusing it to a drug-responsive domain (DRD), such as a destabilized domain (DD) that can act as a degron, thereby inducing conditional degradation of the entire fusion protein via the

[1]Obsidian Therapeutics, Cambridge, MA, USA. [2]These authors contributed equally: Jan ter Meulen, Dhruv K. Sethi. e-mail: dsethi@obsidiantx.com

proteasome[7]. Using the FK506 (tacrolimus) binding protein 12 (FKBP12) and the synthetic ligand Shield-1 in an experimental system, it was shown that the degron activity can be reversibly regulated in a dose-dependent manner[7]. While this system has proved useful as a research tool, Shield-1 is not an FDA-approved drug and other ligands such as tacrolimus or rapamycin have a very narrow therapeutic index making translation into a therapeutic setting challenging. To this end, DDs have been developed that are based on the *E. coli* dihydrofolate reductase (ecDHFR), responsive to the FDA-approved small-molecule antibiotic trimethoprim[8]. While attractive due to the stabilizing ligand used, regulation systems based on non-human components have limited utility because of immunogenicity concerns[9]. Based on these observations we hypothesized that if the human enzyme carbonic anhydrase 2 (CA2) could be engineered to function as a DRD with the ability to be reversibly regulated by the FDA-approved CA2 inhibitor acetazolamide (ACZ), it would be readily translatable to the clinic. ACZ binds tightly to CA2 with low nanomolar affinity and reaches total concentrations in the micromolar range in plasma and other tissues when given at approved doses[10,11]. ACZ is a diuretic, mainly used to treat glaucoma and altitude sickness, and is available as an oral formulation with well-established safety and tolerability[12,13], making a CA2-DRD stabilized by ACZ an excellent candidate for potential clinical translation.

Here, we show that a CA2-derived DRD can regulate the levels of intracellular, secreted, or membrane-bound proteins. The importance of effective regulation of cytokine levels has been noted previously, where IL12, even though regulated by an activation-dependent promoter, still resulted in clinical toxicities[14]. Therefore, to optimize the basal drug-OFF state (no ACZ) of the DRD system, as well as the dynamic range (with ACZ), we multimerized DRD-fused membrane-bound cytokines with naturally occurring intracellular, intramembrane, or extracellular dimerization or trimerization domains, resulting in enhanced degradation and low basal drug-OFF states, while fully preserving cytokine function. Using homologous and heterologous multimerization domains, we generated "modulation hubs" with distinct expression levels and ACZ-dependent regulation kinetics. These modulation hubs can serve as the foundational technology for optimal regulation of a variety of membrane-bound cytokines in T cells, notably IL2, IL12, IL15, IL21, and IL23, which are of prime interest in engineered T cells for ACT[1,15].

Results

A cell-based screening process identifies CA2 variants with drug-responsive stability

To engineer CA2-DRD variants that demonstrate reversible drug-responsive stability, we constructed cell-based libraries of CA2 variants fused to green fluorescent protein (GFP) or mouse Thy1.2 that were subjected to several rounds of functional screening (Fig. 1a). We used a combination of structure-guided design, saturation, and random mutagenesis to create a library of CA2-GFP or CA2-Thy1.2 DNA sequences, which were delivered to cell lines by lentiviral transduction. Stable cell pools were generated through either antibiotic selection or fluorescence-activated cell sorting (FACS) depending on the transduction marker used for a particular library. Iterative cell sorting was used to enrich for library members with low GFP or Thy1.2 expression in the absence of drug (*ACZ-OFF*) and high GFP or Thy1.2 expression in the presence of drug (*ACZ-ON*). After several rounds of cell sorting, the final library was examined through clonal sequencing and/or single-cell cloning. Individual variants were characterized and ranked based on low expression in the drug-OFF state and high dynamic range between drug-OFF and -ON states.

Lead candidates were then further characterized and the EC_{50} value for ACZ stabilization of CA2-DRD GFP fusion was determined (Fig. 1b, c). Viral copy number and transgene RNA expression were measured to ensure similar copy number and transcription levels between cell lines (Supplementary Fig. 1). The EC_{50} of ACZ stabilization of GFP using the characterized CA2-DRDs ranged from 1.6 to 6.43 μM, which is a higher concentration than the potency of inhibition (Ki=12 nM) of wildtype (WT) CA2 activity previously reported[11]. However, EC_{50} and EC_{90} of stabilization are well below total in vivo exposure levels of ~100 μM achieved by FDA-approved and clinically used doses of ACZ[10,16] and CA2-DRDs are expected to be fully stabilized at these concentrations. In addition, other known CA2 inhibitors and drugs known to have off-target activity on CA2 were also capable of stabilizing CA2-DRDs with varying levels of potency (Supplementary Fig. 2), but not considered lead candidates due to discontinuation (ethoxzolamide), insufficient potency (celecoxib), or only non-systemic approved usage (brinzolamide).

Notably, the maximum GFP fluorescence levels for DRD variants were around 45% of WT CA2-GFP, which may indicate some remaining destabilization that cannot be fully rescued by ligand binding. To determine whether the observed differences in basal (*ACZ-OFF*) expression state and EC_{50} differences between variants were related to the stability of the fusion protein, we measured the half-life of the CA2-GFP fusion proteins through drug withdrawal experiments. Cell lines expressing one of two CA2 variants (L156H and S56N) were treated for 24 h with a saturating level of drug to reach a maximum steady-state level of protein. Drug was then withdrawn and WT CA2 was included in the media to act as a sink to bind any residual ACZ as it exited the cells, such that a diffusion gradient favoring more complete elimination from cells was created. GFP fluorescence levels were measured at different time points for 24 h. We observed that the L156H variant with a lower abundance of GFP in the *ACZ-OFF* state and higher EC_{50} had a shorter half-life (4.3 h) than the S56N variant (8.6 h). This suggests that a higher EC_{50} and lower protein levels in the *ACZ OFF*-state are associated with a more destabilized protein (Supplementary Fig. 3).

Degradation of the DRD fusion protein by the proteasome has been implicated as the mechanism of action of DRDs, including those based on ecDHFR and estrogen receptor (ER)[17,18]. To determine if CA2-DRD also functions through similar mechanisms, transduced cells were treated with ACZ for 24 h to fully stabilize the GFP. After culturing for an additional 4 h in the absence of ACZ, cells treated with proteasome inhibitor (MG132) had a smaller decrease in GFP levels than cells cultured in plain media with a vehicle control, demonstrating that proteasomal activity was involved in degrading the DRD fusion protein (Supplementary Fig. 4, reduction of GFP signal in ACZ/dimethyl sulfoxide (DMSO)/proteasome-MG132 group).

The ACZ-bound structure of the CA2-S56N-DRD shows disorder in a loop adjacent to the S56N mutation

To obtain insight into the molecular functioning of the CA2-based DRDs, we set out to crystallize CA2-DRDs in the ACZ-liganded and unliganded states. Despite our best effort, we could obtain crystals only for the CA2 (S56N) DRD in the ACZ-liganded state. The co-crystal structure of CA2 (S56N) was determined to a resolution of 1.79 Å and compared to the structure of WT CA2 complexed to zinc and ACZ (PDB ID 3HS4). Overall, the structure of the CA2 (S56N) mutant is very similar to that of WT CA2 and the Cα root mean square deviation (RMSD) of the two structures is 0.41 Å. The ACZ molecule bound to the WT and CA2 (S56N) mutant is perfectly superimposed and identically coordinates the zinc in the binding site (Supplementary Fig. 5a), which demonstrates that the mutagenesis did not affect the ACZ binding site. However, in the S56N mutant the N56 side chain flips out into the solvent (Supplementary Fig. 5b), which leads to reconfiguration of the existing hydrogen bonding network around the residue (Supplementary Fig. 5c, d; detailed in the Supplementary section), and ultimately leads to destabilization of a loop encompassing residues D71 through A77 (Supplementary Fig. 6a). This loop lies adjacent to the strand bearing the S56N mutation associated with the DRD function and the disorder manifests as missing electron density (Supplementary Fig. 6a). Of note, this residual disorder persists in the presence of ACZ stabilization.

Since the structure of the unliganded S56N mutant CA2 could not be visualized, we cannot speculate as to the extent of the disorder in the overall molecule or in the loop adjacent to the S56N mutation in the unliganded state. To understand the nature of our DRDs and to complement our liganded crystal structure we undertook molecular dynamics (MD) simulations of liganded and unliganded S56N mutant CA2 and compared them to simulations of liganded and unliganded structures of WT CA2

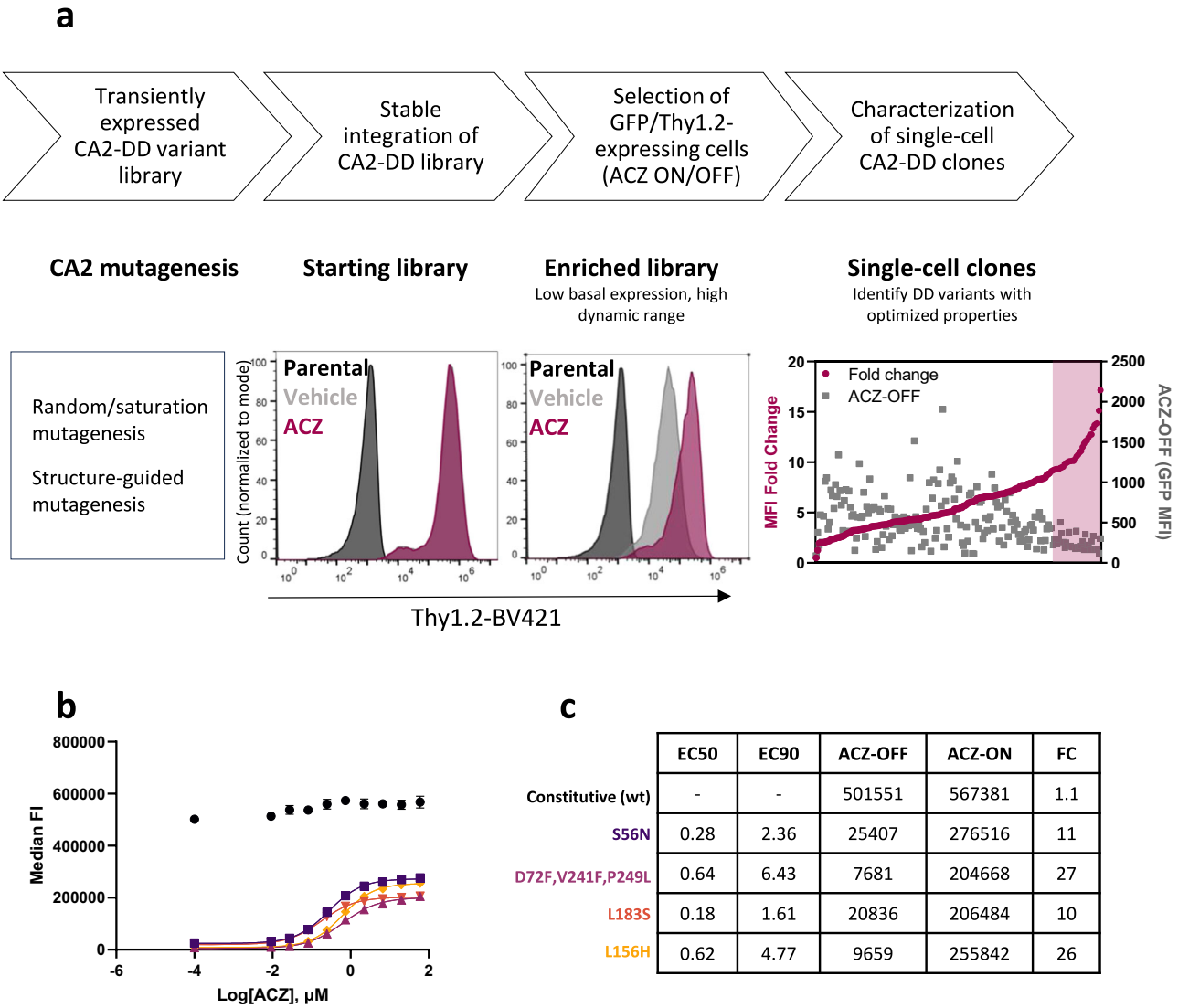

	EC50	EC90	ACZ-OFF	ACZ-ON	FC
Constitutive (wt)	-	-	501551	567381	1.1
S56N	0.28	2.36	25407	276516	11
D72F,V241F,P249L	0.64	6.43	7681	204668	27
L183S	0.18	1.61	20836	206484	10
L156H	0.62	4.77	9659	255842	26

Fig. 1 | Cell-based screening process identifies CA2-DRD variants with drug-responsive stability. a Variant libraries were generated through a combination of random and/or saturation mutagenesis and structure-guided engineering. DNA libraries were fused to a GFP or Thy1.2 expression cassette and integrated into Jurkat cells via lentiviral transduction. Iterative fluorescence-activated cell sorting was used to select for library members showing ACZ ligand-dependent expression of GFP or Thy1.2. Once an enriched library with desired characteristics was obtained, single-cell sorting was used to identify CA2-DRD variants with favorable properties (low basal expression, high dynamic range) for further characterization. Representative library data from CA2-Thy1.2 screen is shown. Characterization of single-cell clones from GFP screen shown. **b** CA2-DRD variants identified by cell-based screening process were fused to GFP and expressed in Jurkat cells by lentiviral transduction. Cells were treated with a range of ACZ concentrations and GFP MFI was measured in transduced cells by flow cytometry. **c** Dose-response curves were used to calculate regulation parameters (EC_{50}, EC_{90}, fold-change [FC= $[GFP\ MFI]_{ACZ}$/$[GFP\ MFI]_{DMSO}$]). Error bars show standard error of the mean ($N = 3$).

(Supplementary Fig. 6b). RMSD was used to determine the difference in the position of the protein backbone compared to the starting structure. The stability of a protein can be determined by the deviations produced during the simulation; smaller deviations indicate greater stability[19]. The unliganded mutant CA2 (S56N) shows the highest amount of flexibility during the MD simulation compared with liganded mutant CA2 and unliganded WT (Supplementary Fig. 6b). Addition of ACZ caused stabilization of the mutant CA2 (S56N) structure as evidenced by the reduction in structural fluctuation, similar stabilization post–ligand-binding has been reported previously for FKBP12-based destabilized domains[20]. The Cα RMSDs of the WT structures in liganded or unliganded forms were very similar in line with the behavior of the WT CA2 in cells. Although, based on the results of the liganded structure and the MD simulation, we cannot state with exactitude what molecular structure CA2 (S56N) adopts when unliganded, the molecule does sample more conformational states than WT CA2 and liganded CA2 (S56N), some of these states might include unstructured regions larger than the loop encompassing residues D71 through K76.

CA2-DRDs regulate expression of various classes of proteins, including membrane-bound cytokines, with differential ACZ-OFF states

After demonstrating the successful regulation of a cytoplasmic protein, GFP, we next fused our lead CA2-DRD (L156H variant) to several other proteins, showing that we can use this domain to regulate expression of intracellular, secreted, membrane-bound, and nuclear proteins (Fig. 2). As an example of an intracellular protein, c-Jun is a transcription factor that forms part of the AP-1 complex and regulates transcription of multiple genes, with transcription activity increasing after phosphorylation of two N-terminal serines and threonines[21–23]. We were able to demonstrate >10× ACZ-regulated expression of c-Jun and ser73-phosphorylated c-Jun (Fig. 2b, c). We were also able to demonstrate regulation of secreted proteins with aflibercept, which is a soluble dimeric glycoprotein and vascular endothelial growth factor (VEGF) antagonist used to treat wet age-related macular degeneration (Fig. 2d, e).

Next, we investigated the use of the CA2-DRD for controlling the expression and activity of pleiotropic cytokines that can amplify the potency

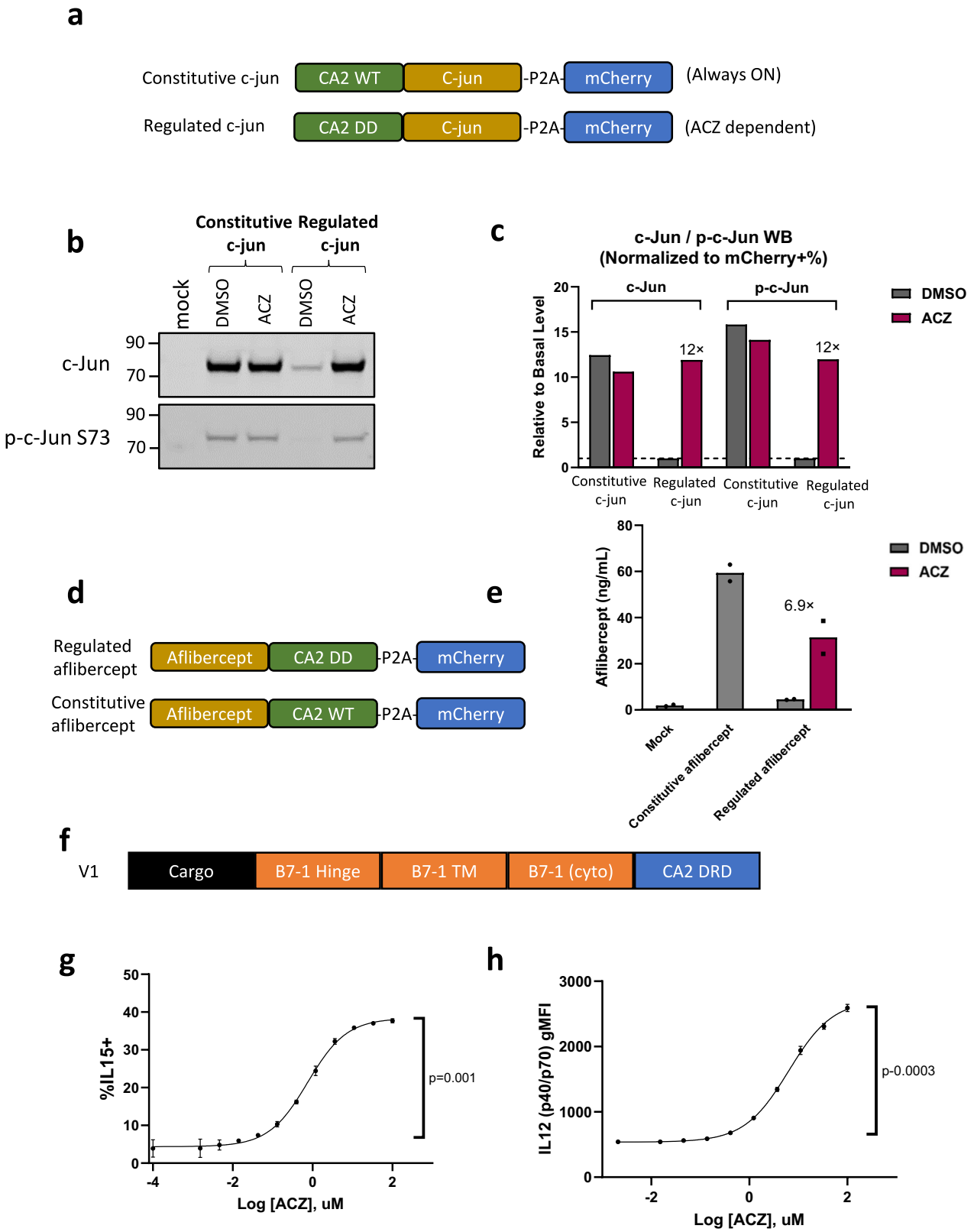

Fig. 2 | CA2-DRD regulates the abundance of different classes of protein in response to ACZ exposure. a Construct schematic of N-terminal CA2-DRD or WT CA2 fused to full-length c-Jun, with mCherry as a transduction marker. **b** Western blot showing detection of c-Jun and phosphorylated c-Jun in presence of DMSO or ACZ in Jurkat cells transduced with constructs 001 or 002. Mock is lysate from empty vector-transduced Jurkat cells. **c** Quantification of the Western blot shown in (**b**). **d** Construct schematic of CA2-DRD or WT CA2 fused to aflibercept. **e** ELISA measurement of secreted aflibercept in the presence of ACZ or DMSO from transfected HEK cells after 24 h of cell culture. Mock sample is supernatant from HEK cells transiently transfected with empty vector. Mock and CA2-wt (constitutive aflibercept) response to ACZ were not measured. Error bars show mean with range ($N = 2$). **f** Construct schematic (labeled as V1) of CA2-DRD–regulated membrane-bound cytokines expressed in Jurkat cells, whose ACZ dose-responses are shown in **g** (IL15) and **h** (IL12). Error bars represent standard deviation ($N = 3$). *P*-values are from a paired two-tailed *T*-Test. The experiments were repeated at least two times with similar results.

of engineered ACT[24]. Membrane-bound cytokines have been shown to retain efficacy while reducing toxicity by limiting systemic exposure[25]. DRDs have the potential to increase safety of cytokines beyond spatially limited activity, due to membrane tethering, by adding a temporal aspect to the expression. Therefore, we sought to create an ACZ-regulated membrane-bound cytokine construct (Fig. 2f, construct format V1), which uses the B7-1 (CD80) transmembrane domain (TM), cytoplasmic domain (cyto), and extracellular hinge. We demonstrated ACZ dose-dependent regulation of membrane-bound IL12 and IL15 with this construct format (Fig. 2g, h), with a maximal induction of ~5-fold over basal (*ACZ-OFF*) expression. We also used the same construct format to regulate membrane-tethered cytokines from other cytokine families (Supplementary Fig. 7). ACZ-dependent increase in expression levels was observed for cytokines from the common gamma chain family (IL2, IL21), IL1 family (IL1β, IL18), and IL12 family (IL23) of cytokines. While we regulated the expression level of all cytokines to some extent, the regulation parameters (EC_{50}, fold-change expression in the *ACZ-ON* over *ACZ-OFF* state) were highly dependent on the protein being regulated, demonstrating the need for optimization. Our ability to regulate membrane-bound cytokines was generally characterized by a low but measurable expression in the *ACZ-OFF* state, and up to a 5-fold dynamic range, except in the case of IL2 and IL21, which showed greater fold induction. (Fig. 2, Supplementary Fig. 7). This range of regulation is sufficient for certain applications; for example, in human plasma, soluble IL15 increased approximately 4-fold in response to a severe systemic bacterial infection, thus the dynamic range of membrane-bound IL15 (mbIL15) regulation in response to ACZ dosing likely mirrors the physiologic regulation of IL15[26]. However, for cytokines like IL12, a much tighter regulation in the drug-OFF state is required to avoid toxicity[27].

Multimerization of CA2 DRD results in improved ACZ-OFF states of regulated proteins with preserved dynamic expression range

We observed that CD40L was well regulated by CA2-DRD (Supplementary Fig. 8). As a member of the tumor necrosis factor superfamily (TNFSF), it occurs naturally in a trimeric state resulting in the presence of three copies of CA2-DRD within each trimer. Therefore, we speculated that DRD multimerization may improve regulation for membrane-bound proteins. To this end, we used protein engineering to generate DRD-cytokine fusion proteins with various transmembrane, cytoplasmic, and hinge sequences, exploring differences in sequence, length, and structural geometries. We tested our initial designs using IL12 as a cargo, and used either the trimerizing motifs from trimeric lectins (collectin-7) or the homo-trimerization domain from collagen 18 to increase the multiplicity of DRDs[28,29] (Fig. 3a–d). Constructs were packaged in lentiviral vectors and transduced into primary T cells at low copy number per transduced cell and protein expression levels were determined by flow cytometry after a 24-hour incubation with DMSO or ACZ (Fig. 3e, f). The basal protein expression in the *ACZ-OFF* state was similar to expression levels in the untransduced cell population, with a robust increase in IL12 expression level in the presence of ACZ (Fig. 3e, f). Further, to reduce the frequency of junction regions in the extracellular regions (to mitigate against potential immunogenicity) we positioned the multimerizing motif of collectin-7 cytoplasmically (Fig. 3g). For similar reasons we also thought to use the transmembrane (TM) from DNAX-activating protein 12 (DAP12), which has a small extracellular domain (ECD) and is capable of forming dimers via disulfide bonds as well as higher-order multimers (trimers and tetramers) via intramembrane charge-charge interactions[30] (Fig. 3h). The construct utilizing the trimerizing helix from collectin-7 to multimerize CA2-DRD continued to regulate IL12 well (16×), even after relocation of the helix into the cytoplasm; also, the use of DAP12 TM to multimerize CA2-DRD significantly reduced the basal *ACZ-OFF* state of protein expression and had robust fold-induction of IL12 expression (10×) (Fig. 3i). Overall, basal protein expression was reduced in the *ACZ-OFF* state and fold-induction of IL12 increased compared with the monomeric DRD fusion construct (Fig. 3i, construct format V1).

In addition to IL12, construct formats V2-V6 (Fig. 4a) were used to induce robust regulated expression of multiple other membrane-bound cytokines. Membrane-bound IFNα, IL23 and IL2 could achieve robust fold-induction with addition of ACZ after being trimerized using the collectin-7 coiled-coil trimerization domain placed cytoplasmically, or by using the DAP12 membrane-spanning helix (Fig. 4b–d). Pentamerization of CA2-DRD–fused cytokines using phospholamban (construct format V6) was also effective in regulating IFNα and IL23. Similar to DAP12, but oriented as a type II transmembrane protein, phospholamban forms stable pentamers within the membrane and does not require any additional intracellular or extracellular multimerization domains[31]. Each of the cytokines IFNα, IL23, IL2, and IL12 had low basal abundance in the *ACZ-OFF* state and robust induction in the *ACZ-ON* state when configured as multimerizing constructs (V2–V6) compared with the non-multimerizing membrane-bound construct format V1 (Fig. 4b–d, Fig. 3i, Fig. 2g). IFNα was similar to IL21 and IL2 (Fig. 3g, h, Supplementary Fig. 7), in having a robust fold-induction (13×; Fig. 4b) in format V1, albeit with a higher basal abundance compared with the multimerizing constructs. Since expression levels of multiple cytokines could be modulated by ACZ using constructs that included multimerizing domains acting as hubs to increase valency of DRDs, we address these types of constructs as "modulation hub" constructs. The regulation of multiple cytokines simply by switching the cytokine cargo highlights the plug-and-play possibilities of this technology.

Since we were positioning these cytokines as dimers or trimers and in several cases expressing them as part of integral type II transmembrane proteins, we wanted to understand whether the cytokines retained their biological function. Constructs IL2-V3 and IL2-V4 (Fig. 4) are designed as type II integral membrane proteins such that the CA2-DRD is positioned at the N-terminus (intracellular) and the IL2 is at the C-terminus (extracellular). Due to the extracellular positioning of trimerization domains in these constructs, IL2 is expressed as a trimer on the cell surface. HEK-blue IL2 reporter cells that secrete embryonic alkaline phosphatase (SEAP) in response to bioactive IL2 through a STAT5 inducible promoter, when co-cultured with Jurkat cells expressing ACZ-regulated membrane-bound IL2, showed that the multimerized IL2 could effectively initiate JAK-STAT signaling in an effector cell dose dependent manner (Fig. 5a, b). The maximum fold-induction of JAK-STAT signaling with ACZ administration was 2.6-fold for IL2-V4, and 2.3-fold for IL2-V3, respectively. Construct IL12-V2 is designed as a type I transmembrane protein that multimerizes via the DAP12 TM (Figs. 3h, 4a), while IL12-V5 is designed as a type II transmembrane protein with multimerization occurring through an intracellular collectin-7 trimerizing helix (Figs. 3g, 4a).

The modulation hub scaffold also presents the opportunity to engineer additional functionality such as induced shedding of the cargo protein. While all the modulation hub constructs contain the metalloprotease cleavage site from CD40L in the hinge, only IL12 was observed to shed in our in vitro experiments. This is likely due to cell polarization induced by IL12 signaling causing upregulation of sheddases[32]. Therefore, the modulation hubs regulate not only cell surface IL12, but also shed IL12 as well as the subsequent JAK-mediated signaling in cells exposed to conditioned media in an ACZ-dependent manner (Fig. 5c, d).

Effects of multimerization on basal protein expression levels can be shown through hetero-trimerization

To show the effect of increasing valency of DRDs on lowering of basal protein abundance in the *ACZ-OFF* state and increasing the level of stabilized protein in the *ACZ-ON* state, we designed an experiment where we could compare regulation by constructs bearing one, two or three copies of the same DRD. DAP12 is an immunoreceptor tyrosine-based activation motif (ITAM)-bearing signal-transducing adapter protein for a number of immune receptors such as KIRs, TREM1/2, NKG2C, CD33, and SIRP1β that are themselves incapable of signal transduction[33–36]. DAP12 can exist in dimeric, trimeric, and tetrameric states[30]; however, in the presence of various other binding partners such as KIRs, it preferentially contributes two parallel TM helices and forms a heterotrimer with an anti-parallel TM helix from one of its binding partners[30]. The TM heterotrimers are stabilized by intramembrane charge-charge interactions similar to those

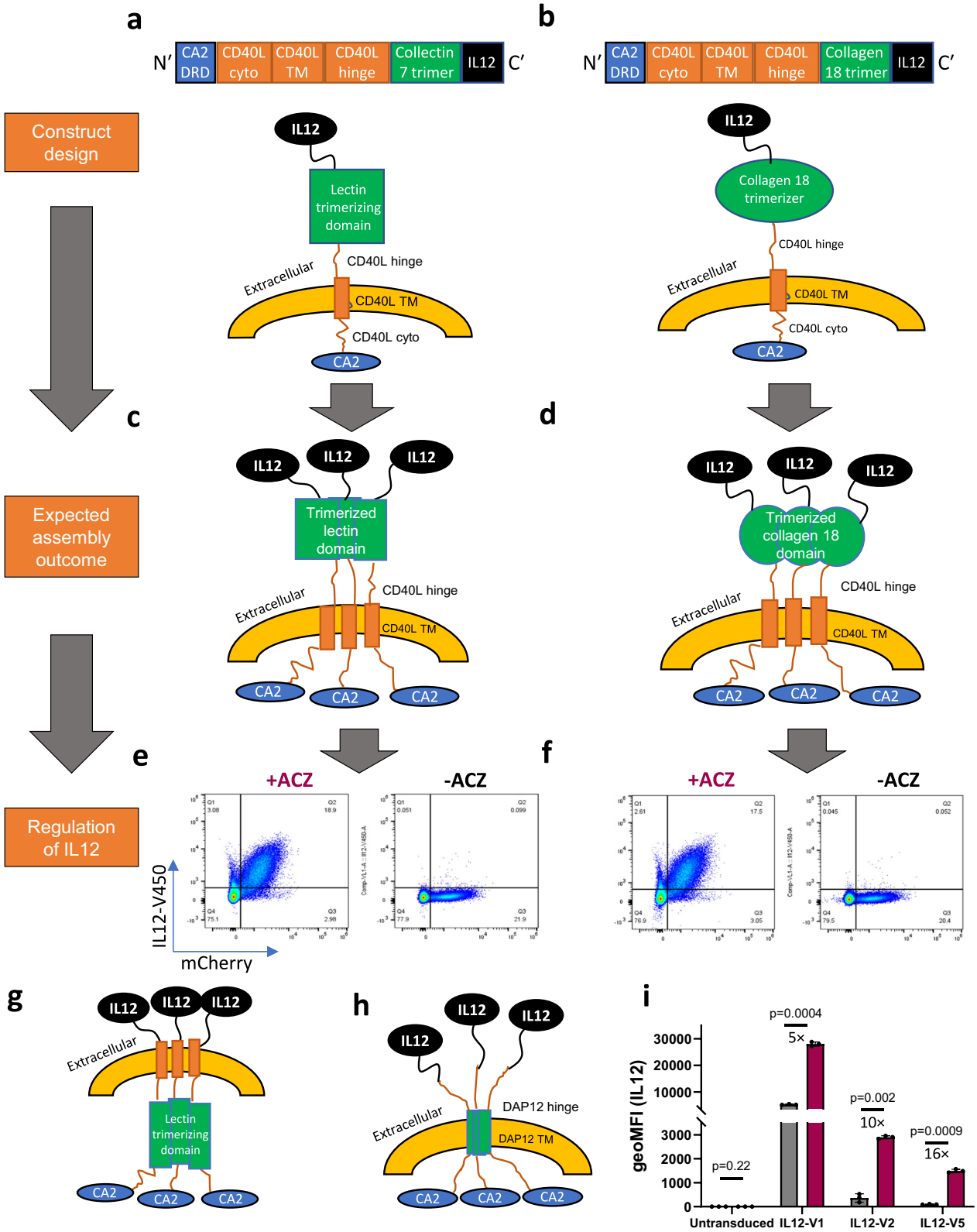

Fig. 3 | Membrane-bound scaffolds that promote multimerization can effectively regulate IL12 abundance. Schematic of designed membrane-bound IL12 constructs using multimerizing domains from (**a**) collectin-7 and (**b**) collagen 18. **c** Putative intracellular assembly of the designed construct shown in (**a**). **d** Putative intracellular assembly of the designed construct shown in (**b**). **e** and **f** Detection of IL12 on Jurkat cell surface in the presence or absence of ACZ. **g** Schematic showing intracellular repositioning of the collectin-7 trimerizing domain. **h** Schematic showing multimerization of IL12 through its TM. **i** Bar graph showing IL12 surface expression levels on T cells in the presence or absence of ACZ for the construct with intracellularly repositioned trimerizing domains as shown in (**g**) and (**h**) and compared with construct format V1. Error bars represent standard deviation ($N = 3$). *P*-values are from a paired two-tailed *T*-Test. The experiments were repeated at least three times with similar results.

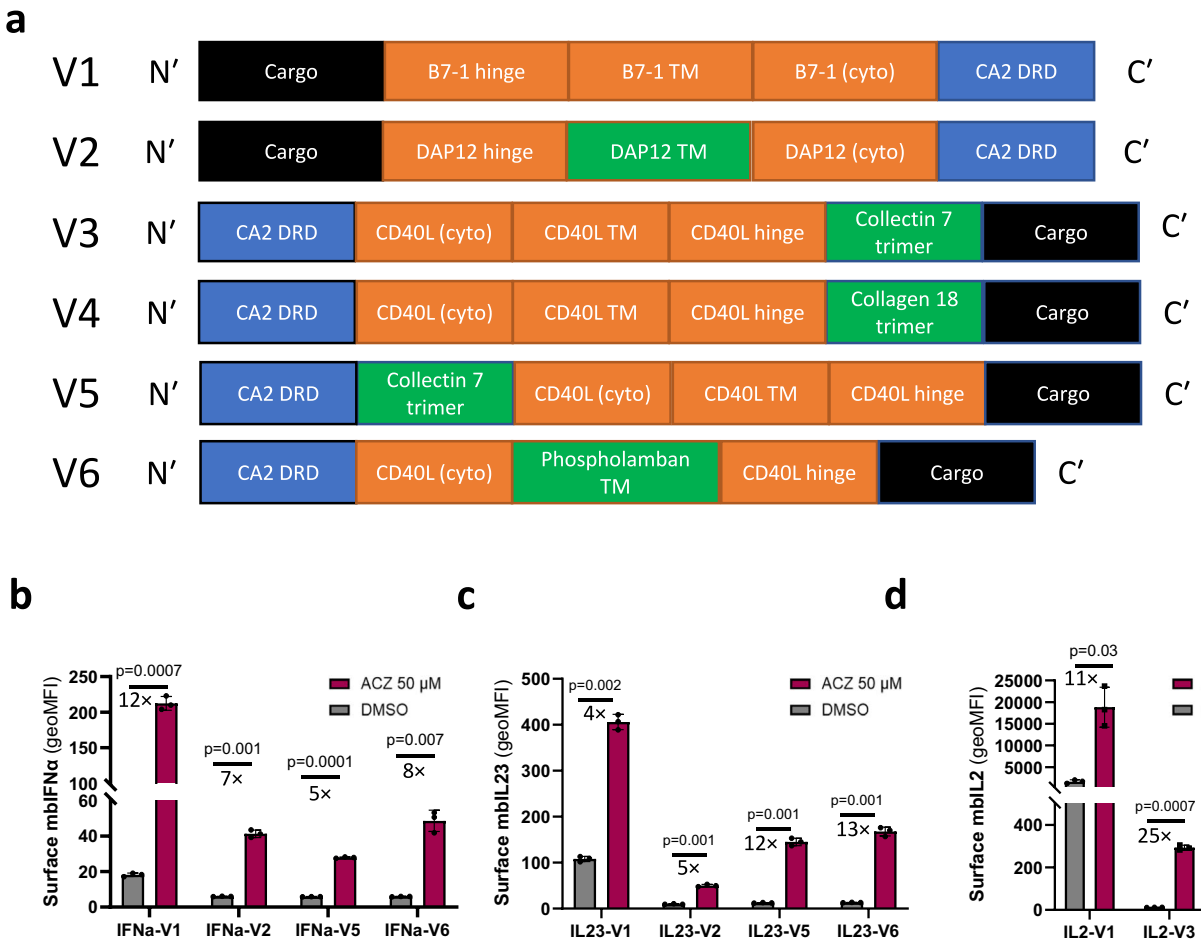

Fig. 4 | Optimized modulation hubs can be used to regulate cell surface expression of a broad range of cytokines. a Schematics of representative constructs (V1–V6) that were used to regulate the surface expression of **b** IFNα, **c** IL23 and **d** IL2 in Jurkat cells. The construct version (V1–V6) used for each of the cytokines is indicated on the x-axis labels. In each schematic the domain responsible for the multimerization is in green, the cargo in black, the DRD in blue and linkers and hinges are highlighted in orange. Error bars represent standard deviation ($N = 3$). *P*-values are from a paired two-tailed *T*-Test. The experiments were repeated at least three times with similar results.

seen in T-cell receptor (TCR) assembly[37]. One of the most well-characterized heterotrimeric TM bundles involving DAP12 is the trimer formed with the NKG2C TM[35] (Fig. 6a). We created a series of constructs where in each instance the cargo (IL12) was appended to the C-terminus of truncated NKG2C hinge (no ECD), while the position of the appended CA2-DRD was varied to generate either 1, 2, or 3 copies in the multimerized construct (Fig. 6b, c). When appended to NKG2C, there is only a single copy, while appended to DAP12, the valency increases to two, and when appended to both DAP12 and NKG2C the valency of CA2-DRD increases to three. Increasing valency of CA2-DRD manifests as a reduction in basal abundance of IL12 on the cell surface in the *ACZ-OFF* state with a concomitant increase in fold–induction of protein expression. We observe similar results using virally transduced Jurkats (Fig. 6d, e), and in transiently transfected HEK293 cells (Fig. 6f, g). Further, an increase in MFI (Fig. 6c, d) is evident in the trimer in the *ACZ-ON* state in Jurkat cells, contributing to a larger fold-change in the heterotrimeric state. Taken together, this demonstrates that multimerization can reduce the drug-OFF–state expression of the DRD fusion protein while maintaining the ability to increase expression and dynamic range in the presence of stabilizing ligand.

CA2 modulation hubs enable IL12-mediated regulated efficacy in a solid tumor model

We next demonstrated the ability of modulation hubs to regulate IL12-mediated efficacy in a solid tumor in vivo model by armoring anti-CD19 chimeric antigen receptor (CAR)-T cells with IL12 (Fig. 7a). Modulation hub construct IL12-V5 was inserted behind the CD19 CAR (Supplementary Fig. 9a). The CAR-T cells were assessed for their ability to produce and regulate IL12 prior to infusion into the mice (Supplementary Fig. 9b). Raji tumor cells (Burkitt's Lymphoma), mixed with Matrigel, were implanted subcutaneously into the right flank of NSG mice and established for 14 days, reaching an average tumor volume greater than 100 mm^3 before adoptive cell transfer (ACT). Mice treated with empty vector engineered T cells succumbed to tumor burden within 3 weeks post-randomization. Unarmored and vehicle-dosed IL12-armored CAR-T cells delayed tumor growth but could not eliminate tumor. 10 million unarmored CAR-T cells were able to control tumor, but mice showed early signs of graft vs host disease 30 days post-ACT and were euthanized. IL12-armored CAR-T cells were able to control tumor burden when dosed with ACZ at a 10-fold lower cell dose than unarmored CAR-T cells (Fig. 7b). Animals dosed with one million IL12-armored CAR-T cells (in the drug-ON state) showed significantly ($p = 0.04$) prolonged survival compared to those who received a one million unarmored CAR-T cell dose (median survival of 40 days versus 21 days, Fig. 7c). Moreover, there was insignificant difference between the one million IL12-armored CAR-T cells (in the drug-OFF state and the one million unarmored CAR-T cell dose ($p = 0.99$). T cells isolated from submandibular bleeds showed higher expression of membrane-bound IL12 in ACZ-treated mice (Fig. 7d, Supplementary Fig. 9c); further, shed IL12 levels in plasma were higher relative to vehicle-treated mice (Fig. 7e). Together these data show that modulation hubs regulate potent cytokines in vivo in

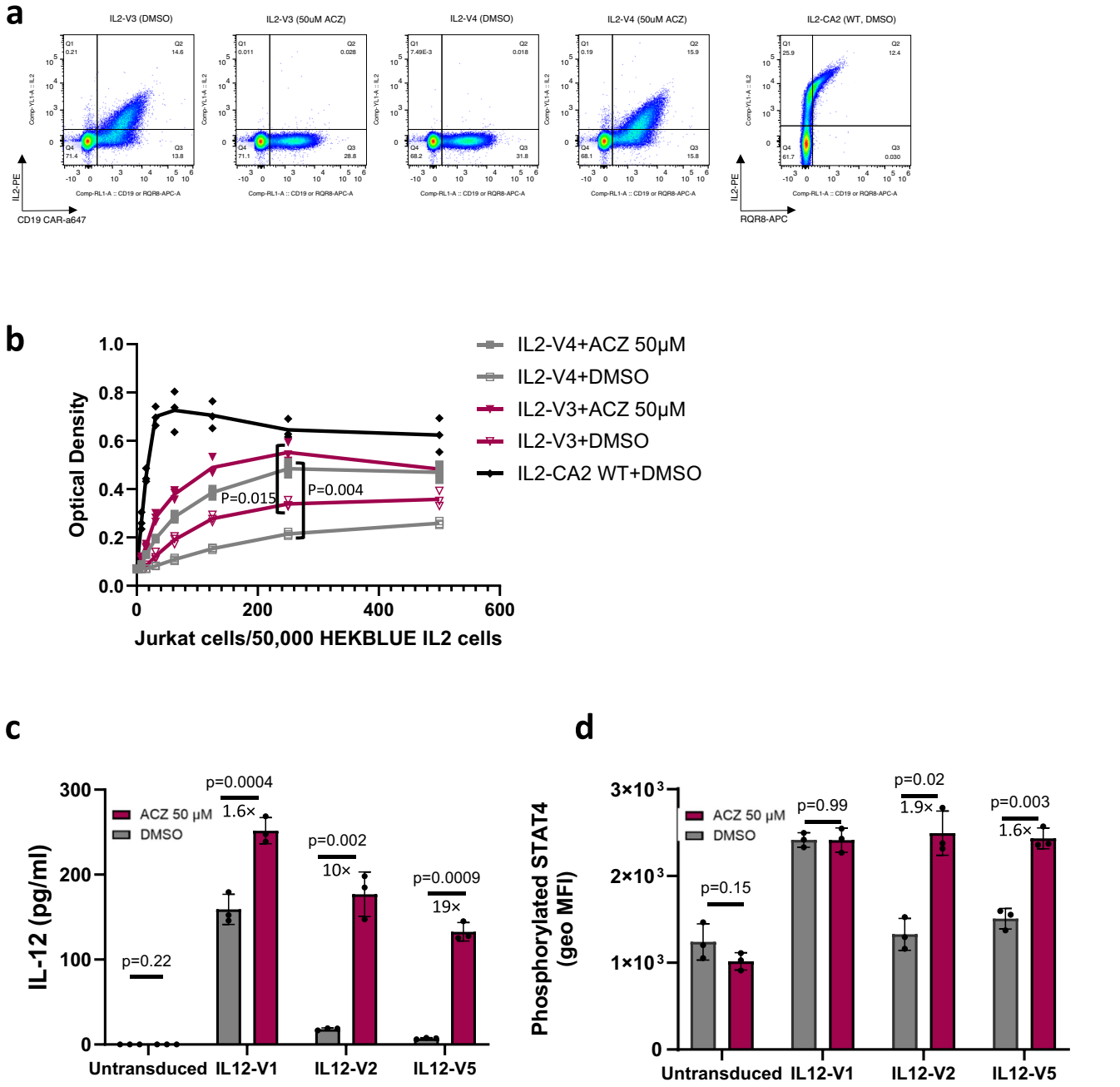

Fig. 5 | Membrane-bound cytokines regulated using multimeric modulation hubs are functional. a Scatter plots demonstrating regulated expression of IL2 in the presence of 50 μM ACZ using two different multimerizing modulation hubs (IL2-V3 and IL2-V4). Membrane-bound IL2 as in construct schematic V1 but fused to WT CA2 is used as a positive control for mbIL2 expression. **b** SEAP levels quantitated at optical density 620 (y-axis) are plotted against number of transduced Jurkat cells for every 50,000 HEK blue (IL2) on the x-axis ($N = 3$, lines connect the means). **c** Shed IL12 levels from untransduced T cells or from IL12 transduced T cells utilizing constructs V1, V2 or V5 in the presence or absence of 20 μM ACZ were measured by MSD assay. **d** Levels of phosphorylated STAT4 in natural killer (NK) cells after being incubated with supernatants from T cells transduced with the same constructs (as in **c**) and exposed to ACZ or DMSO control were measured by flow cytometry. Error bars represent the standard deviation ($N = 3$). *P*-values are from a paired two-tailed *T*-Test. The experiments were repeated three times with similar results.

armored CAR-T cells enabling regulated efficacy and survival in a solid tumor setting.

Discussion

The purpose of the work presented here was to design and optimize a regulation technology for potent membrane-tethered cytokines in engineered cell therapies targeting solid tumors. DRDs are ideal for this application as they: (1) allow for rapid induction of target protein activity in the presence of a stabilizing small-molecule drug and (2) enable rapid turnover of the target protein via the proteasome in the absence of stabilizing drug. Previously transcribed mRNA is translated into protein that can be stabilized co-translationally in the presence of the drug; therefore, rapid accumulation of protein occurs when drug is present. Further, unlike transcriptional and pre-transcriptional regulation where protein half-life is innate to the protein, DRDs act as degrons that rapidly shorten the half-life of proteins after drug withdrawal, the rate-limiting step being stability of the DRD-drug complex. Together, these enable a temporally regulated drug-ON system that can be used to manage levels of potent cytokines as needed. Additionally, DRDs are small domains fused directly to the protein of interest, simplifying their use via viral gene delivery compared to multi-component systems[38].

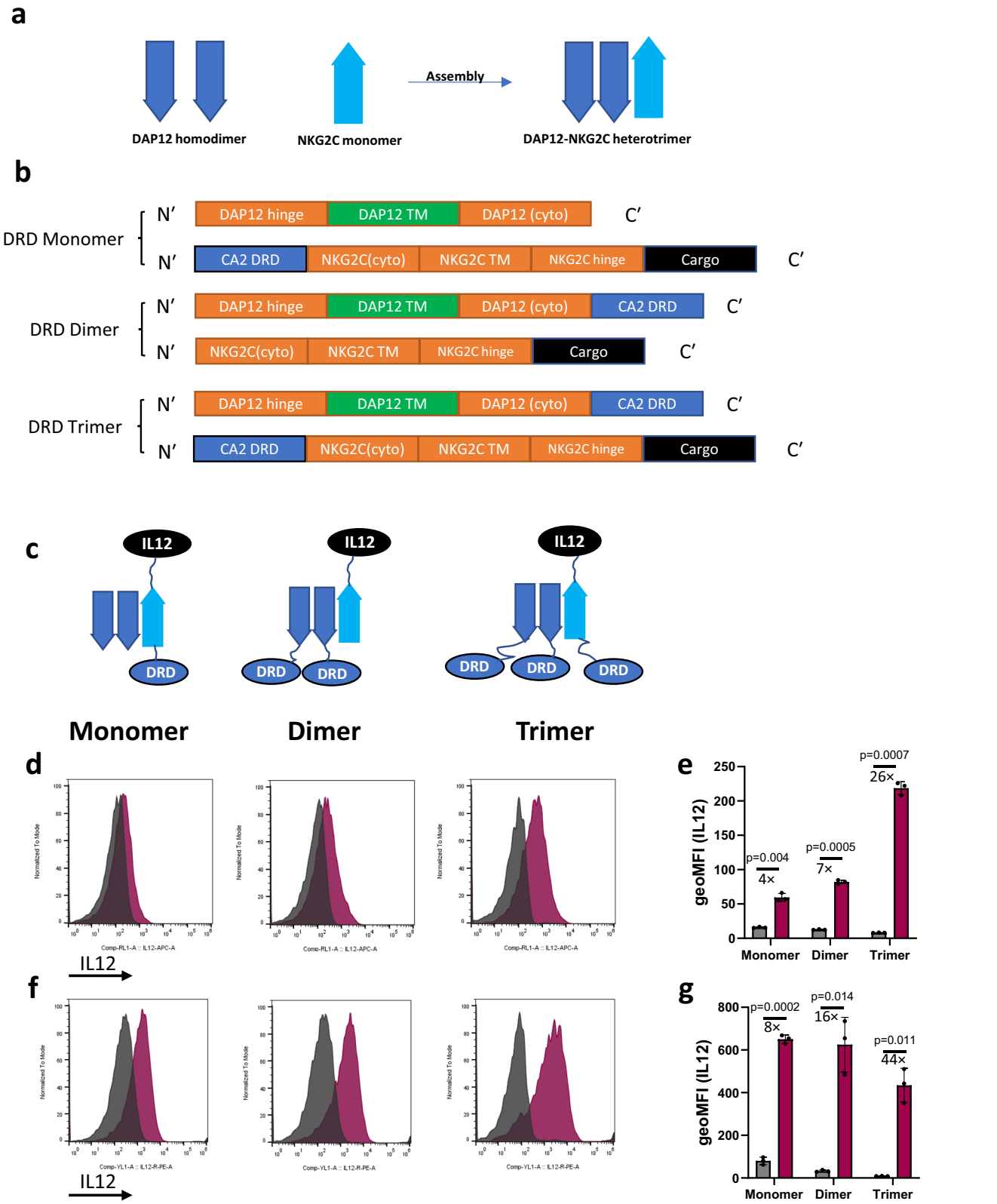

Fig. 6 | DRD multimerization using scaffolds decreases basal abundance and increases dynamic range of regulation of protein expression. a Representation of the helices of DAP12 and NKG2C showing relative orientations in assembled heterotrimer. **b** Schematics of proteins that were co-expressed to generate either a DRD monomer, dimer, or trimer. **c** Representations of predicted assembled constructs representing the monomeric, dimeric, and trimeric DRD assemblies. **d** Overlaid histograms showing IL12 levels on cell surface of transduced Jurkat cells with DMSO (gray) and after addition of ACZ (magenta) as measured by flow cytometry. **e** Quantitation of IL12 MFI of the histograms in (**d**) DMSO (gray), ACZ (magenta). Reduction in basal and increasing fold-induction was also seen in transiently transfected HEK293 cells. **f** Overlaid histograms showing IL12 levels on cell surface with DMSO (gray) and after addition of ACZ (magenta) measured by flow cytometry. **g** Quantitation of IL12 MFI of the histograms in (**f**) DMSO (gray), ACZ (magenta), the error bars in (**e**, **g**) represent the standard deviation ($N = 3$). *P*-values are reported from a paired two-tailed *T*-Test. The experiments were repeated at least three times with similar results.

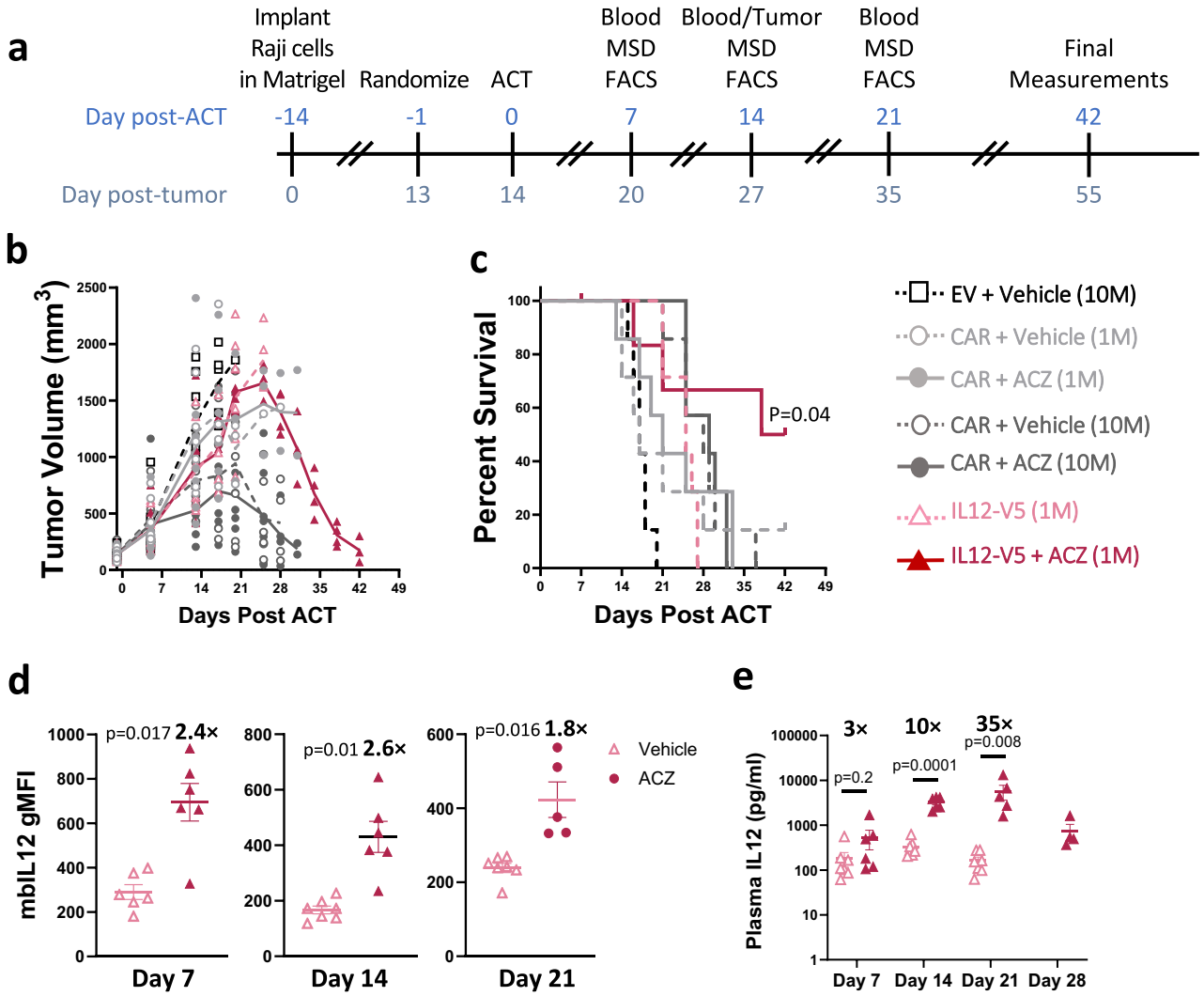

Fig. 7 | CAR-T cells armored with CA2 DRD regulatable IL12 show ACZ dependent efficacy. a Time course of the subcutaneous Raji model. **b** Mean tumor volumes of mice throughout the study ($N = 7$, lines connect the means). **c** Percent survival of mice from all groups. **d** Ex-vivo analysis of mbIL12 levels on the surface of CAR+ cells on day 7, 14 and 21 for DRD-regulated mbIL12-armored T cells in the no ACZ group (light pink) and the ACZ group (dark pink). **e** Quantitation of IL12 levels in the plasma of mice on day 7, 14, 21 and 28. **f** Number of CAR-T cells/mL of blood in various groups on days 7, 14, 21 and 28. Survival statistics analyzed in GraphPad Prism using Mantel-Cox test. *P*-values reported for data in (**d**, **e**), are from an unpaired *T*-Test.

We constructed a DRD from the human enzyme CA2 to act as a degron in the absence of its stabilizing ligand, ACZ. Our strategy of using a fully human DRD coupled with an FDA-approved small molecule aims to reduce regulatory hurdles as compared to using a non-human, likely immunogenic, protein coupled with a non–FDA-approved small molecule, as often used in other regulation systems[6]. ACZ was approved in the US in 1954 as a mild diuretic and is currently mainly used to treat glaucoma and prevent altitude sickness[12,13]. Careful selection of small molecule drugs to regulate the cargo of interest is very important as illustrated by the recent example of the non–FDA-approved molecule branaplam (LMI070), which was used as the ligand in a recently described alternate splicing-based regulation system (Xon)[39]. The clinical trial in which branaplam was tested for treatment of Huntington's disease had to be halted because of drug-related side effects[40].

To obtain a suite of DRDs that responded to ACZ, we followed a functional screening strategy similar to that used earlier to discover destabilized domains[7,8]. To increase throughput, we attempted to use in silico methods, including Monte Carlo-based methods and machine learning to predict reversible destabilizing mutations that can be stabilized by ACZ. These efforts, however, met with limited success, as the small fraction of the predicted and tested mutations that showed DRD-like behavior were invariably inferior to the mutants identified through the functional screening method. The reasons behind this might be two-fold; first, there is still significant imprecision in protein structure prediction and second, the inability to model cellular processes such as the interaction of the DRD with chaperones or the proteasome[41]. As an example of the former, in the Alphafold2 model of the S56N mutant the asparagine side chain is modeled as continuing to point toward the protein core (Supplementary Fig. 10). Nevertheless, trends in relative instability of DDs have been correlated with biophysical observations[20]. To understand the structural correlates of CA2 DRD function we sought to obtain the structures of liganded and unliganded CA2 DRDs. Several CA2 DRDs could be produced and purified as recombinant proteins; however, we succeeded only in obtaining crystals and determining the structure of CA2 (S56N) bound to ACZ. The unliganded CA2 (S56N) could not be crystallized. This can likely be explained by differences in stability of the non-liganded and ACZ-stabilized states of the various DRD mutants, where the S56N mutant shows evidence of slower degradation kinetics than the L156H mutant after drug withdrawal, leading to higher protein abundance in both the presence and absence of ACZ (Supplementary Fig. 3). The crystal structure of liganded CA2 (S56N) shows that the N56 side chain flips out into the solvent and a stretch of five residues in an adjacent loop has high thermal mobility and inadequate electron

density, demonstrating that some residual disorder persists in the ACZ-bound structure[42].

In the unliganded state FKBP12 DRDs have been shown to exist in partially to fully unfolded states, which are associated with poly-ubiquitination and proteasomal degradation, and drug binding causes the protein domain to adopt a more stable fold[20]. In this respect, the co-crystal structure of CA2 (S56N) and ACZ represents the more stable liganded fold. Although we cannot comment on the exact structural nature of the unliganded protein, our MD simulations do show that the unliganded CA2 (S56N) is more flexible than the liganded mutant and the liganded/unliganded WT protein. This suggests that CA2 (S56N) might also function as a DRD by similar mechanisms as FKBP12, possessing a much greater degree of disorder corresponding to unfolded states in the absence of drug. A correlation between the presence of disordered regions and protein half-life is well known, with the presence of unstructured regions being important for proteasomal degradation[43]. The stretch of disordered residues that persists after ligand binding might explain why the GFP MFI at maximal stabilization is only 45% of a WT CA2 and GFP fusion.

Membrane tethering of cytokines with or without the potential to be shed in the desired environment is a potential strategy to make use of the immunostimulatory function of cytokines while limiting their systemic toxicity and has been pursued with IL12, IL15, and IL21 engineering mainly of NK cells and CAR-T cells[25,44]. Our initial attempts at tightly regulating membrane-bound cytokines with a CA2 DRD resulted in most cytokines being regulated only modestly, with the basal expression in the ACZ-OFF state being relatively high and dynamic range of regulation less than 10-fold. It is important to note that the plasma levels of secreted cytokines are generally low (single- to low-double digit pg/mL) in a healthy state, while the dynamic range of expression can vary from several-fold in immune activation to several log-fold in disease states with cytokine release syndrome[26,45]. In an engineered ACT, baseline expression of certain potentially toxic cytokines (e.g., IL12) in the absence of stabilizing drug will be amplified as the engineered cells expand in the patient; therefore, it is more critical to have tight regulation over the baseline expression than a large dynamic range. To this end, we explored molecular design strategies to improve regulation of membrane-bound proteins.

Increasing the multiplicity of DRDs by fusing them simultaneously to both N- and C-termini of the target protein has been shown to improve regulation compared to a single fusion at either terminus[46]; indeed, increased dynamic range has been observed as number of FKBP DRDs increased from one to three; however, fusing at both termini can compromise function[47]. The increased fold-induction and reduced basal expression in the drug-OFF state is likely sequence- and context-dependent, as increasing the copies of FKBP-DRDs from one through three at the C-terminus of YFP, for example, showed the opposite phenotype[48]. Our method of increasing DRD multiplicity using multimerizing domains has the distinct advantage of optimizing vector capacity, as only a single coding sequence produces the multiplicity of DRDs needed to improve control. Using our hetero-trimerization approach we furthermore showed that increasing valency of DRDs reduces the basal abundance of the cargo proportionally. We conjecture that increasing the valency of degrons attached to the cargo might make them more effective targets for recruitment to the proteasome, by increasing the frequency of such recruitment post-translationally. Having a well-characterized panel of multimerization domains is critical to be able to effectively regulate expression of a variety of cytokines.

Since IL2 and IL12 are not normally membrane-bound or multimerized, it was pivotal to confirm that these modifications do not interfere with their ability to activate downstream signaling and to be able to show that such function was selectively enhanced in the presence of ACZ. We demonstrate cytokine function is preserved not only in vitro, but that ACZ dependent expression enhances functionality in vivo. Overall, our data demonstrate that DRD multimerization significantly lowers the drug-OFF state and thereby increases the drug-dependent dynamic range of expression of membrane-bound cytokines without compromising biological function.

Despite the impressive successes of cancer immunotherapy in the past decade, complete responses are obtained only in a small subset of solid tumors, primarily those with a high mutational burden and pre-existing infiltration of immune cells[49]. A major obstacle to achieving better outcomes for patients is the immunosuppressive nature of the TME, which prevents the establishment of effective antitumor immune responses by multiple mechanisms involving checkpoint-mediated exhaustion of immune cells, induction of regulatory cells, remodeling of the vascular bed and stromal architecture, and others[50]. Pro-inflammatory cytokines are attractive therapeutic tools that can remodel the TME and induce infiltration and activation of multiple antitumor immune cells, such as T cells, NK cells, macrophages, and dendritic cells, as well as impact stromal cells and endothelial cells[3,51]. However, their clinical use is restricted by systemic toxicity, especially that of the potent cytokines IL2 and IL12[1]. With the CA2-DRD and a suite of DRD modulation hubs that allow us to fine-tune the regulation of expression of a broad range of cytokines, we have unlocked the capability to engineer more powerful cell therapies while maintaining tight regulation of their activity through an FDA-approved drug at clinically approved dosages. OBX-115, our lead experimental tumor-infiltrating lymphocyte cell therapy candidate expressing ACZ-regulated mbIL15 is showing promising results in a Phase 1 clinical trial (NCT05470283) in patients with metastatic melanoma, and a Phase 1/2 clinical trial is recruiting patients with metastatic melanoma and non-small cell lung cancer (NCT06060613)[52].

Materials and methods

Construct generation

Random mutagenesis library of full-length CA2 was generated at GenScript by error-prone PCR using nucleotide analogs, 7-one-5-triphosphate (dPTP) (TriLink) and 8-oxo-dGTP (TriLink), mediated mutagenesis[53]. CA2 random mutagenesis library was ligated into a pLVX-Puro lentivirus plasmid backbone (Clontech) containing EF1a promoter driven Aequorea coerulescens GFP (AcGFP) to generate pLVX-AcGFP-CA2 library. Alternatively, saturation mutagenesis library of CA2 was produced by Ranomics and assembled downstream of AcGFP into a pLVX lentivirus vector containing AcGFP-P2A-mCherry using Gibson assembly reagents (NEB). Finally, a saturation mutagenesis library of CD8a signal-peptide fused CA2 was assembled upstream of a Furin site fused to mouse Thy1.2 followed by P2A-mCherry into a pELNS lentivirus backbone. For each type of library (random mutagenesis and saturation mutagenesis), control plasmid was generated by inserting WT CA2 rather than the mutagenesis library.

For expression of CA2-regulated proteins-of-interest by transduction as lentivirus vectors, plasmids were each constructed in a pELNS vector (a third-generation self-inactivating lentiviral expression vector) using standard molecular biology techniques. Gene fragments (Gblocks or strings DNA) encoding various cargoes, glycine-serine linkers, various hinges, TM domains and cytoplasmic tails were purchased from Integrated DNA Technologies or Thermo-Fisher Scientific. The gene fragments were inserted into the pELNS vector and placed under the control of the EF1a promoter using Gibson assembly (NEBuilder Hifi). The assembled plasmid was transformed into *E. coli* (NEB stable) for amplification and sequence confirmed before proceeding with virus production.

AcGFP-CA2 or CA2-Thy1.2 cell line generation and characterization

For random mutagenesis library plasmids, saturation mutagenesis CA2 library plasmids, and corresponding control plasmids were packaged into VSV-G pseudotyped lentivirus. For random mutagenesis library NIH3T3 cells were transduced and for saturation mutagenesis Jurkat cells were transduced with the mutant library or control virus at a low multiplicity of infection (MOI) to ensure low copy number of transgene per cell. Cells were

expanded and transduced cells were selected either using Puromycin or by sorting for mCherry marker expression.

Flow cytometry

Antibodies specific for appropriate surface markers (Table 1) were combined in a mixture at appropriate dilutions (20× to 100×) and 50 µl added to cell pellets in V-bottom 96-well plates for 25-30 minutes of staining at room temperature followed by 2 washes with 150 µL of FACS buffer. If secondary staining was required, then the process was repeated with anti-Fc reagents. An AttuneNXT (Life Technology) or Symphony (BD) flow cytometers were used to acquire data before analyzing using FlowJo software (BD).

Western blot

Transduced cells were seeded in 6-well plates at 1×10^6 cells/mL and treated with DMSO or ACZ (100 µM) for 24 h. Cells were washed once with cold PBS and lysed in 120 µL IP lysis buffer. Protein was quantified by BCA assay (Pierce) and 20 µg total protein were loaded per lane of a 4−12% Bis-Tris mini protein gel (Invitrogen). Chameleon® Duo Pre-stained Protein Ladder (Licor) was loaded as a size marker. Protein was transferred using iBlot 2 (Life Technologies) and membranes were stained in iBind system (Life Technologies). Primary antibodies were c-Jun (CST #9165 Rabbit) Green 1:1,1000, Phospho-c-Jun S73 (CST #3270 Rabbit) Green 1:1,000, or Tubulin (Sigma T5168 Mouse) Red 1:4,000. Secondary antibodies were IRDye® 800CW Donkey anti-Mouse IgG (Licor, 926-32212), or IRDye® 680RD Donkey anti-Rabbit IgG (Licor, 926-68073) diluted according to iBind directions. Stained membranes were imaged using Licor Odyssey DLx (Licor).

Table 1 | Flow cytometry reagents

Antigen	Fluorophore	Vendor	Catalogue Number	Dilution
IL12 P40	V-450	BD	561380	1:100
IL12 P40	PE	BioLegend	501807	1:100
IL2	APC	BioLegend	500311	1:100
IFNa	PE	BD	560097	1:100
IL1b	FITC	BioLegend	511705	1:100
IL18/IL1F4	Unconjugated - Mouse IgG	Novus	925008	1:100
Anti-Mouse IgG	AF647	Jackson Immunoresearch	115-605-071	
IL21	APC	ThermoFisher	17-7211-82	1:100
Live/Dead Dye	NIR	eBioscience	65-0865-14	1:100
Human FC-Block	Unconjugated	BioLegend	422302	1:100
CD56	FITC	BioLegend	318304	1:100
CD3	PE-Cy7	BioLegend	344816	1:100
pSTAT4	PE	BD	562074	1:20
IL12 P70	PE	BD	559325	1:100
CD19-Fc	Unconjugated, Human Fc fusion	R&D Systems	9269-CD	1:200
CD34/RQR8	APC	R&D Systems	FAB7227A	1:100
Thy1.2	BV421	BioLfegend	105341	1:100
Anti-Human IgG	BV421	BioLegend	409318	1:200
FACS buffer		BD	420201	
Counting Beads		BioLegend	424902	

Antigen: IL2; Fluorophore:PE; Vendor: Invitrogen; Catalogue Number:12-7029-42; Dlution 1:50.

DRD screen by sorting

Transduction marker-selected cells were used for multiple rounds of iterative sorting to select for cells that express AcGFP or Thy1.2 when treated with ACZ (SelleckChem) and do not express AcGFP or Thy1.2 when treated with vehicle (DMSO). Before each round of sorting, cells were characterized by treating with ACZ or DMSO and collecting 24 h post-treatment to observe GFP expression by FACS. Cells expressing CA2-Thy1.2 were stained for Thy1.2 expression. The top or bottom 10-40% of GFP or Thy1.2 expressing cells (gated on single cells) were isolated in alternating sequential sorts to obtain a population that was enriched for increased expression of GFP or Thy1.2 in response to drug treatment using the SH800 cell sorter (Sony).

Library sequencing and cell line characterization

After 3 rounds of sorting, the enriched cells were collected, and genomic DNA was extracted (QIAGEN). Using primers specific to sequences flanking the CA2 sequence in the library, the mutant CA2 sequence remaining in the cell population was amplified with Q5 Hot Start polymerase (ThermoFisher). These sequences were inserted into the original AcGFP-P2A-mCherry vector digested with BcuI and Esp3I (ThermoFisher) using T4 DNA ligase (NEB). Assembled library plasmid was transformed, and colonies were Sanger sequenced using primers flanking CA2 sequence. The sequences that had highest representation in the population were packaged into lentivirus and Jurkat cell lines were generated through transduction. These cells were treated with ACZ (SelleckChem), ethoxzolamide (SelleckChem), brinzolamide (SelleckChem), celecoxib (SelleckChem), or topiramate (SelleckChem) for 24 h and characterized by FACS using AttuneNXT cytometer (LifeTechnology). Dose-response curves were generated on GraphPad Prism.

To measure vector copy number (VCN), DNA was isolated using the DNeasy kit (Qiagen). Copy number of WPRE was measured by qPCR using Taqman assays (IDT) on a Quantstudio 6 (Applied Biosystems). Ct values were calculated using the Quantstudio software. To calculate copy number per cell, a standard curve was used to covert Ct to copies and this was normalized to RPPH1 gene (assumed to have 2 copies/cell). To measure gene expression from the integrated construct, RNA was isolated from cell lines using RNeasy (Qiagen). Relative expression of WPRE normalized to RPPH1 (2^-ΔΔCt) was compared across cell lines. Expression of WPRE and RPPH1 were measured using Taqman assays (IDT, WPRE: Forward: CCGTTGTCAGGCAACGTG, Reverse: AGCTGACAGGTGGTGGCAAT, Probe (FAM): TGCTGACG CAACCCCCACTGGT; RPPH1 Forward: ACTTTTTCCCATAGGGC GGAGG, Reverse: TCTGGCCCTAGTCTCAGACCTT, Probe (HEX): CCACGAGCTGAGTGCGTCCTGT) and qScript XLT One-Step RT-qPCR ToughMix (QuantaBio).

Proteasome inhibition assay

Jurkat cells transduced with CA2-DRD constructs were plated in 96-well plates at 5E5 cells/mL in 200 µL and treated with either DMSO or 20 µM ACZ (Selleck Chemicals) for 24 h. After 24 h, cells were washed with fresh media and split into 2 groups that either continued initial treatment conditions or added 10 µM MG132 (Selleck Chemicals) in addition to initial treatment for 4 h. Expression of GFP was measured by flow cytometry using the Attune NxT (ThermoFisher Scientific).

Structure determination

CA2 (S56N) fused to a 9× His-tag was cloned into pET21b and expressed in *E. coli*. Protein was purified using a NiNTA column and was further purified using size exclusion chromatography using a superdex 75 column (Cytiva) after cleavage by ULP1 to remove the 9× His-tag. Purified protein was concentrated to 6.7 mg/mL and utilized for crystallization. Crystals were obtained in 1.45 M sodium citrate, 0.1 M Tris-HCl pH 8.0, 4% v/v

polypropylene glycol P 400. Crystals were cryoprotected using 20% glycerol and data were collected at Diamond synchrotron, Beamline I03 to a resolution of 1.79 Å. Structure was determined using PDB ID 3DC3 as the probe and model building and refinement was performed using Coot (WinCoot 0.9.8.1)[54] and refmac5[55]. Data collection and refinement statistics are presented in Table 2. Molecular graphics representations and structural analyses were generated using PyMOL (v2.6.0a0 open source). The crystal structure of ACZ-bound CA2 (S56N) has been deposited in the PDB with accession code 8VZG.

MD simulations

Atomistic MD simulations were performed using the GROMACS 2022.3 software package[56], the AMBER99SB-ILDN force field and the TIP3P three-point water model. Ligands were parameterized using ACPYPE and GAFF as a force field[57]. MD simulations on the mutant CA2 (S56N), utilized the determined crystal structure described in this paper as the starting model, while the CA2 (WT) simulations utilized PDB entry 3HS4 as the starting model. In the process of building the complete system, the protein-ligand complex was placed in a box of cubic form filled with a solvent with a physiological concentration of NaCl (0.15 M), total charge of the system was equal to zero. The distance between the complex and the walls of the box was kept at 10 Å. Periodic boundary conditions were used in these simulations. Electrostatic energy was calculated using the PME (Particle-Mesh Ewald) method. Coulomb and van der Waals interactions had a limiting distance of 1.0 nm. The energy minimization was carried out using the steepest descent algorithm to a system energy value of <1000 kJ/mol/nm (50,000 steps maximum). Equilibration was carried out in two consecutive phases, with positional restraints on the protein and ACZ (for the S56N + ACZ simulation). The temperature was equilibrated to a temperature of 300 K (100 ps) using a modified Berendson thermostat (v-rescale) and the pressure to 1 atm (150 ps) using c-rescale. Equilibration was confirmed by monitoring the temperature during NVT equilibration and pressure during NPT equilibration (Supplementary Fig. 13). The production MD simulations were carried out without positional restraints for 50 ns, with a time step of 2 fs, starting with random initial velocities. RMSD of atomic coordinates during the simulation from their respective initial coordinates were calculated using the gmx_rms tool, while radius of gyration was calculated using the gyrate functionality in Gromacs. MD simulations were repeated three times starting from randomized initial velocities with similar results. An overview of the MD simulations is provided in Supplementary table 1.

Table 2 | Data collection and refinement statistics

	Crystal 1
Data collection	
Space group	P212121
Cell dimensions	
a, *b*, *c* (Å)	42.53, 69.04, 80.07
a, b, g (°)	90, 90, 90
Resolution (Å)	29.15–1.79 (1.83–1.79)[a]
R_{sym} or R_{merge}	0.090 (0.676)
I / s*I*	18.3 (2.3)
Completeness (%)	99.1 (88.4)
Redundancy	11.7 (7.0)
Refinement	
Resolution (Å)	29.15–1.79
No. reflections	21582
R_{work} / R_{free}	0.15 / 0.181
No. atoms	
Protein	2084
ACZ	13
Ion	2
GOL	18
FLC	13
Water	206
B-factors	
Protein	24.073
ACZ	18.6
Ion	17.71
GOL	36.39
FLC	27.6
Water	34.79
R.m.s. deviations	
Bond lengths (Å)	0.0091
Bond angles (°)	1.7749

[a]Ranges in parentheses refer to the highest resolution shell.

Cell culture, transfection, and transduction

NIH3T3 cells (ATCC) were cultured in high glucose DMEM (Life Technologies) supplemented with 10% Donor Bovine Serum (DBS; Life Technologies), 1% glutamine (Life Technologies). HEK293T cells (ATCC) were cultured in high glucose DMEM (Life Technologies) supplemented with 10% heat-inactivated FBS (Life Technologies). HEK293 were transfected with plasmids using Lipofectamine 3000 (Life Technologies) following manufacturers protocol. Cells were analyzed 48 h post-transfection in the presence or absence of ACZ. Appropriate antibodies, listed in Table 1 were used to detect expression of cargo.

Jurkat, Clone E6-1, cells were cultured in standard media (RPMI+ GlutaMAX Supplement: Life Technologies Cat# 61870127, Fetal Bovine Serum [FBS] Life Technologies Cat# 10-082-147). Jurkat cells were transduced with lentivirus to 10–25% positive as determined by using mCherry as a transduction marker. Five days post-transduction, the cells were treated with 100 µM ACZ or DMSO and the cells were further cultured for 1 more day. Appropriate antibodies, listed in Table 1 were used to detect expression of cargo. For constructs which did not have a transduction marker, mock stained untransduced cells were used to set the positive gate to determine the percent positive population.

On day 0, primary human T cells were stimulated with Dynabeads (T-expander CD3/CD28; Thermo Fisher Scientific) at a 3:1 bead: cell ratio in media containing 10% FBS. The next day, lentivirus supernatants were added in the presence of reduced serum (5% FBS). On day 2, the cells were diluted 1:2 with fresh 10% FBS media. On day 5, the cells were analyzed for transduction efficiency using flow cytometry. Media was replaced and cells were treated with 25 µM or 50 µM ACZ or DMSO. Twenty-four hours later, T cells were assessed for expression of cargo using cargo appropriate antibodies as listed in Table 1.

STAT4 assay

Upon IL12 engagement with its receptors, STAT4 becomes phosphorylated and serves as a proximal readout of IL12 activity. NK cells isolated from peripheral blood mononuclear cells were thawed from liquid nitrogen storage and rested overnight. Supernatants (100 µL) from IL12-transduced cells were added to 40,000 NK cells in 100 µL of media. The NK cells were assessed for STAT4 phosphorylation after 1 h of incubation with the IL12-containing supernatants. Viability dye and human Fc block were added to the cells during the last 10 min of the incubation. Cells were spun at 400 RCF for 5 min, pellets resuspended in 200 µL of 37 C 1× fixation buffer (BD Cat# 558049) and incubated at 37 C for 10 min. Plates were spun and placed on ice before resuspending with 100 µL of ice-cold Buffer III (BD Cat# 558050) for 30 min in the dark. Plates were washed 2× with 150 µL FACs buffer before adding surface (CD56 and CD3) and pSTAT4 antibodies for 45 min

at room temperature in the dark. Cells were washed twice with 150 µL of FACS buffer before analysis with NK cells (defined as CD56+CD3-).

HEK-blue assay for IL2 activity

The HEK-blue 293 IL2 and IL15 reporter cell line was acquired from Invivogen (Cat#hkbil2). Jurkat cells transduced with IL2-V3 and IL2-V4 or IL2-V1 (with $CA2^{WT}$) were normalized using untransduced Jurkat cells and mixed at 10:1, 5:1, 2.5:1, 1.25:1, 1:1.6, 1:3.2 and 1:6.4 ratio with 50,000 HEK blue IL2 cells in 200 µL media. After a 24-h co-culture the supernatant was collected and 20 µL of supernatant was used to quantitate the amount of secreted embryonic alkaline phosphatase (SEAP). Plates were read at 620 nm after 3 h of incubation with QUANTIblue reagent (Invivogen Cat. #rep-qbs) at 37 °C. IL2-V3 and V4 used CD19CAR as a transduction marker, while IL2-V1 (with $CA2^{WT}$) used RQR8 as a transduction marker.

CD19-CAR expansion for in vivo studies

On day 0, primary human T cells were stimulated with Dynabeads (T-expander CD3/CD28; Thermo Fisher Scientific) at a 3:1 bead: cell ratio in media. The next day, lentivirus supernatants were added. On day 2, the cells were diluted 1:3 with fresh media. On day 4, replicate wells were combined, debeaded, and added to 10 M Grex wells (Wilson Wolf 80110) in a total volume of 100 mL. Human IL2 was added to a final concentration of 10 ng/mL (R&D Systems, 202-IL) on days 4 and 9. Cells were harvested on day 14 and frozen in CS10 (StemCell technologies, 7930). Cells were thawed and assessed for CAR expression using flow cytometry. 50,000 CD19-CAR+ cells from thawed cells were added to 96 well V-bottom plates and restimulated with CD3/28 (StemCell ImmunoCult Cat# 10971) and 20 µM ACZ before assessing for cytokine production and pSTAT4 activity as described above. Shed cytokine levels were quantitated using V-PLEX IL12p70 meso scale discovery kit (MSD Kit K15049D). On day of ACT, cells were thawed and resuspended in PBS at an appropriate concentration for a 100 µL injection volume/mouse.

Raji cell culture

Raji cells were acquired from ATCC, Catalog # CRL-2631. Cells were cultured in complete media of RPMI 1640 + GlutaMax (Gibco; Catalog #61870-036) with 10% Heat-inactivated Fetal Bovine Serum (Gibco; Catalog #10082-147) and incubated at 37 °C, 5% CO_2. On the day of implant, cells were counted, washed, and resuspended at a concentration of 50×10^6/mL in a 1:1 suspension of sterile PBS (Gibco; Catalog #10010-023) and Matrigel (Corning; catalog #356234).

Subcutaneous Raji model

Five to six-week-old female NSG mice (NOD.Cg-Prkdc Il2rg/SzJ mice, Part# 005557) were obtained from Jackson Laboratory (Bar Harbor, ME). On day 0, mice were anesthetized briefly under 3% Isoflurane with 1.5% O_2; right flanks were shaved, and 100 µL (5×10^6 cells) cells were injected subcutaneously.

Animals were randomized into groups based on an approximate mean tumor volume of 150 mm^3 on day 13 post subcutaneous Raji tumor cell implant. On day 14, mice were infused with the corresponding CAR-T/T cells to their study group via tail vein injection. Immediately after adoptive cell transfer (ACT), mice were dosed with the corresponding ligand to their study group (+ ACZ) via oral gavage and followed a daily dosing regimen until the completion of the study. Mice were caliper measured and weighed twice weekly for the duration of the experiment. Once per week, blood was harvested via cheek bleeds for flow cytometric analysis of whole blood and cytokine concentration in the plasma (MSD Kit K15049D). All mouse experiments were approved by the Obsidian Therapeutics Institutional Animal Care and Use Committee.

Statistics and reproducibility

Information about statistical analyses, the number of experimental replicates, p values are specified within the main text, figure legends, figures or methods. Unless otherwise stated, data are shown as mean ± SD and p-values are from a paired two-tailed T-Test performed in excel. Significance of the survival shown in Fig. 7c was analyzed in GraphPad Prism 10 using the Mantel-Cox test. An unpaired t-test was performed on data shown in Fig. 7d, e, using GraphPad Prism 10.

Reporting summary

Further information on research design is available in the Nature Portfolio Reporting Summary linked to this article.

Data availability

The authors declare that all data supporting the findings in this study are available within the article or within the supplementary data. Source data and all other data can be obtained from the corresponding author on reasonable request. The crystal structure of ACZ bound CA2 (S56N) has been deposited in the PDB with accession code 8VZG. Full western blot images are shown in Supplementary Fig. 12.

Received: 5 March 2024; Accepted: 17 December 2024;
Published online: 09 January 2025

References

1. Berraondo, P. et al. Cytokines in Clinical Cancer Immunotherapy. *Br. J. Cancer* **120**, 6–15 (2019).
2. Kagoya, Y. Cytokine signaling in chimeric antigen receptor t cell therapy. *Int. Immunol*. **2023**, dxad033. https://doi.org/10.1093/intimm/dxad033.
3. Etxeberria, I. et al. Engineering Bionic T Cells: Signal 1, Signal 2, Signal 3, reprogramming and the removal of inhibitory mechanisms. *Cell. Mol. Immunol.* **17**, 576–586 (2020).
4. Zhang, P., Zhang, G. & Wan, X. Challenges and new technologies in adoptive cell therapy. *J. Hematol. Oncol. J. Hematol. Oncol.* **16**, 97 (2023).
5. Di Stasi, A. et al. Inducible apoptosis as a safety switch for adoptive cell therapy. *N. Engl. J. Med.* **365**, 1673–1683 (2011).
6. Nadendla, K. et al. Strategies for conditional regulation of proteins. https://doi.org/10.17863/CAM.95852 (2023).
7. Banaszynski, L. A., Chen, L., Maynard-Smith, L. A., Ooi, A. G. L. & Wandless, T. J. A rapid, reversible, and tunable method to regulate protein function in living cells using synthetic small molecules. *Cell* **126**, 995–1004 (2006).
8. Iwamoto, M., Björklund, T., Lundberg, C., Kirik, D. & Wandless, T. J. A general chemical method to regulate protein stability in the mammalian central nervous system. *Chem. Biol.* **17**, 981–988 (2010).
9. Latta-Mahieu, M. et al. Gene transfer of a chimeric trans-activator is immunogenic and results in short-lived transgene expression. *Hum. Gene Ther.* **13**, 1611–1620 (2002).
10. Ritschel, W. A. et al. Pharmacokinetics of Acetazolamide in Healthy Volunteers after Short- and Long-Term Exposure to High Altitude. *J. Clin. Pharmacol.* **38**, 533–539 (1998).
11. Carta, F. & Supuran, C. T. Diuretics with carbonic anhydrase inhibitory action: a patent and literature review (2005 – 2013). *Expert Opin. Ther. Pat.* **23**, 681–691 (2013).
12. Schmickl, C. N., Owens, R. L., Orr, J. E., Edwards, B. A. & Malhotra, A. Side effects of Acetazolamide: a systematic review and meta-analysis assessing overall risk and dose dependence. *BMJ Open Respir. Res.* **7**, e000557 (2020).
13. Kassamali, R. & Sica, D. A. Acetazolamide: a forgotten diuretic agent. *Cardiol. Rev.* **19**, 276–278 (2011).
14. Zhang, L. et al. Tumor-infiltrating lymphocytes genetically engineered with an inducible gene encoding Interleukin-12 for the immunotherapy of metastatic melanoma. *Clin. Cancer Res.* **21**, 2278–2288 (2015).
15. Wang, J., Johnston, B. & Berraondo, P. Editorial: cytokine and cytokine receptor-based immunotherapies: updates, controversies, challenges, and future perspectives. *Front. Immunol.* **13**, 985326 (2022).

16. Tsikas, D. Acetazolamide and human carbonic anhydrases: retrospect, review and discussion of an intimate relationship. *J. Enzym. Inhib. Med. Chem.* **39**, 2291336 (2024).
17. Miyazaki, Y., Imoto, H., Chen, L. & Wandless, T. J. Destabilizing domains derived from the human estrogen receptor. *J. Am. Chem. Soc.* **134**, 3942–3945 (2012).
18. Nakahara, E., Mullapudi, V., Collier, G. E., Joachimiak, L. A. & Hulleman, J. D. Development of a New DHFR-based destabilizing domain with enhanced basal turnover and applicability in mammalian systems. *ACS Chem. Biol.* **17**, 2877–2889 (2022).
19. Aier, I., Varadwaj, P. K. & Raj, U. Structural insights into conformational stability of both wild-type and mutant EZH2 receptor. *Sci. Rep.* **6**, 34984 (2016).
20. Egeler, E. L., Urner, L. M., Rakhit, R., Liu, C. W. & Wandless, T. J. Ligand-switchable substrates for a Ubiquitin-proteasome system. *J. Biol. Chem.* **286**, 31328–31336 (2011).
21. Baumann, S. et al. An unexpected role for FosB in activation-induced cell death of T cells. *Oncogene* **22**, 1333–1339 (2003).
22. Wang, L., Gao, J., Dai, W. & Lu, L. Activation of Polo-like Kinase 3 by Hypoxic stresses. *J. Biol. Chem.* **283**, 25928–25935 (2008).
23. Nateri, A. S., Spencer-Dene, B. & Behrens, A. Interaction of phosphorylated C-Jun with TCF4 regulates intestinal cancer development. *Nature* **437**, 281–285 (2005).
24. Allen, G. M. et al. Synthetic cytokine circuits that drive T cells into immune-excluded tumors. *Science* **378**, eaba1624 (2022).
25. Pan, W.-Y. et al. Cancer immunotherapy using a membrane-bound interleukin-12 With B7-1 transmembrane and cytoplasmic domains. *Mol. Ther.* **20**, 927–937 (2012).
26. Lauw, F. N. et al. Elevated plasma concentrations of interferon (IFN)–γ and the IFN-γ–Inducing Cytokines Interleukin (IL)–18, IL-12, and IL-15 in severe melioidosis. *J. Infect. Dis.* **180**, 1878–1885 (1999).
27. Jia, Z. et al. IL12 immune therapy clinical trial review: novel strategies for avoiding CRS-Associated Cytokines. *Front. Immunol.* **13**, 952231 (2022).
28. Kovacs, H. et al. Solution structure of the coiled-coil trimerization domain from lung surfactant protein D. *J. Biomol. NMR* **24**, 89–102 (2002).
29. Boudko, S. P. et al. Crystal structure of human collagen XVIII trimerization domain: a novel collagen trimerization fold. *J. Mol. Biol.* **392**, 787–802 (2009).
30. Knoblich, K. et al. Transmembrane complexes of DAP12 crystallized in lipid membranes provide insights into control of oligomerization in immunoreceptor assembly. *Cell Rep.* **11**, 1184–1192 (2015).
31. Becucci, L. et al. On the function of pentameric phospholamban: ion channel or storage form? *Biophys. J.* **96**, L60–L62 (2009).
32. Chowdhury, F. Z., Ramos, H. J., Davis, L. S., Forman, J. & Farrar, J. D. IL-12 selectively programs effector pathways that are stably expressed in human CD8+ effector memory T cells in vivo. *Blood* **118**, 3890–3900 (2011).
33. Haure-Mirande, J.-V., Audrain, M., Ehrlich, M. E. & Gandy, S. Microglial TYROBP/DAP12 in Alzheimer's disease: transduction of physiological and pathological signals across TREM2. *Mol. Neurodegener.* **17**, 55 (2022).
34. Mulrooney, T. J., Posch, P. E. & Hurley, C. K. DAP12 impacts trafficking and surface stability of killer immunoglobulin-like receptors on natural killer cells. *J. Leukoc. Biol.* **94**, 301–313 (2013).
35. Call, M. E., Wucherpfennig, K. W. & Chou, J. J. The structural basis for intramembrane assembly of an activating immunoreceptor complex. *Nat. Immunol.* **11**, 1023–1029 (2010).
36. Lanier, L. L., Corliss, B. C., Wu, J., Leong, C. & Phillips, J. H. Immunoreceptor DAP12 Bearing a Tyrosine-Based activation motif is involved in activating NK cells. *Nature* **391**, 703–707 (1998).
37. Feng, J., Call, M. E. & Wucherpfennig, K. W. The assembly of diverse immune receptors is focused on a polar membrane-embedded interaction site. *PLoS Biol.* **4**, e142 (2006).
38. Leung, W.-H. et al. Sensitive and adaptable pharmacological control of CAR T cells through extracellular receptor dimerization. *JCI Insight* **4**, e124430 (2019).
39. Monteys, A. M. et al. Regulated control of gene therapies by drug-induced splicing. *Nature* **596**, 291–295 (2021).
40. Novartis. Community Update: Status of VIBRANT-HD, the Study of Branaplam/LMI070 in Huntington's Disease, 2022. https://hdsa.org/wp-content/uploads/2022/12/Novartis-VIBRANT-HD-Community-Letter-FINAL-PDF.pdf.
41. Fraser, J. S. & Murcko, M. A. Structure is beauty, but not always truth. *Cell* **1870**, 517–520 (2024).
42. Piovesan, D. et al. DisProt 7.0: a major update of the database of disordered proteins. *Nucleic Acids Res.* **45**, D219–D227 (2017).
43. van der Lee, R. et al. Intrinsically disordered segments affect protein half-life in the cell and during evolution. *Cell Rep.* **8**, 1832–1844 (2014).
44. Nguyen, R. et al. Cooperative armoring of CAR and TCR T Cells by T Cell–Restricted IL15 and IL21 Universally enhances solid tumor efficacy. *Clin. Cancer Res*. OF1–OF12.https://doi.org/10.1158/1078-0432.CCR-23-1872. (2023).
45. Liu, C. et al. Cytokines: from clinical significance to quantification. *Adv. Sci.* **8**, 2004433 (2021).
46. Maji, B. et al. Multidimensional chemical control of CRISPR–Cas9. *Nat. Chem. Biol.* **13**, 9–11 (2017).
47. Qi, Z. et al. An optimized, broadly applicable *piggyBac* transposon induction system. *Nucleic Acids Res*. **45**, e55 (2017).
48. Chu, B. W., Banaszynski, L. A., Chen, L. & Wandless, T. J. Recent progress with FKBP-Derived destabilizing domains. *Bioorg. Med. Chem. Lett.* **18**, 5941–5944 (2008).
49. Cristescu, R. et al. Tumor mutational burden predicts the efficacy of pembrolizumab monotherapy: a pan-tumor retrospective analysis of participants with advanced solid tumors. *J. Immunother. Cancer* **10**, e003091 (2022).
50. De Visser, K. E. & Joyce, J. A. The evolving tumor microenvironment: from cancer initiation to metastatic outgrowth. *Cancer Cell* **41**, 374–403 (2023).
51. Rossari, F., Birocchi, F., Naldini, L. & Coltella, N. Gene-Based delivery of immune-activating cytokines for cancer treatment. *Trends Mol. Med.* **29**, 329–342 (2023).
52. Wickwire, J. *Obsidian Therapeutics Announces Positive Interim Top-Line Clinical Data for OBX-115 Engineered TIL Cell Therapy in Advanced or Metastatic Melanoma Post-Anti-PD1 Therapy*.; Press release. https://obsidiantx.com/news-releases/obsidian-therapeutics-announces-positive-interim-top-line-clinical-data-for-obx-115-engineered-til-cell-therapy-in-advanced-or-metastatic-melanoma-post-anti-pd1-therapy/.
53. Zaccolo, M., Williams, D. M., Brown, D. M. & Gherardi, E. An approach to random mutagenesis of DNA using mixtures of triphosphate derivatives of nucleoside analogues. *J. Mol. Biol.* **255**, 589–603 (1996).
54. Emsley, P., Lohkamp, B., Scott, W. G. & Cowtan, K. Features and development of coot. *Acta Crystallogr. D. Biol. Crystallogr.* **66**, 486–501 (2010).
55. Murshudov, G. N., Vagin, A. A. & Dodson, E. J. Refinement of macromolecular structures by the maximum-likelihood method. *Acta Crystallogr. D. Biol. Crystallogr.* **53**, 240–255 (1997).
56. Van Der Spoel, D. et al. GROMACS: fast, flexible, and free. *J. Comput. Chem.* **26**, 1701–1718 (2005).
57. Sousa Da Silva, A. W. & Vranken, W. F. ACPYPE - AnteChamber PYthon Parser interfacE. *BMC Res. Notes* **5**, 367 (2012).

Author contributions

D.K.S. and J.T.M. supervised the project. D.K.S., M.C.I., J.T.M., and J.T. conceived the project and designed the experiments. S.S., D.L., B.P., D.S., G.O., K.S., T.R., M.L., V.Y., A.A., S.D., J.G., M.S., and M.C.I. performed and analyzed experiments. D.K.S., M.C.I., J.T.M., J.T.. and M.O. interpreted the results and wrote the paper.

Competing interests

The authors declare the following competing interests: all authors are, or were at the time of performing the work, full-time employees and shareholders of Obsidian Therapeutics.

Additional information

Supplementary information The online version contains supplementary material available at https://doi.org/10.1038/s42003-024-07410-z.

Correspondence and requests for materials should be addressed to Dhruv K. Sethi.

Peer review information *Communications Biology* thanks Yuki Kagoya, and the other, anonymous, reviewers for their contribution to the peer review of this work. Primary Handling Editors: Guideng Li and Laura Rodríguez Pérez. A peer review file is available.